BIPOLAR ORIENTATIONS ON PLANAR MAPS AND SLE_{12}

By Richard Kenyon, Jason Miller, Scott Sheffield and David B. Wilson

We give bijections between bipolar-oriented (acyclic with unique source and sink) planar maps and certain random walks, which show that the uniformly random bipolar-oriented planar map, decorated by the "peano curve" surrounding the tree of left-most paths to the sink, converges in law with respect to the peanosphere topology to a $\sqrt{4/3}$-Liouville quantum gravity surface decorated by an independent Schramm-Loewner evolution with parameter $\kappa = 12$ (i.e., SLE_{12}). This result is universal in the sense that it holds for bipolar-oriented triangulations, quadrangulations, k-angulations, and maps in which face sizes are mixed.

CONTENTS

1. Introduction.

1.1. *Planar maps.* A *planar map* is a planar graph together with an embedding into $\mathbb{R}^2$ so that no two edges cross. More precisely, a planar map is an equivalence class of such embedded graphs, where two embedded graphs are said to be equivalent if there exists an orientation preserving homeomorphism $\mathbb{R}^2 \to \mathbb{R}^2$ which takes the first to the second. The enumeration of planar maps started in the 1960's in work of Tutte [70], Mullin [57], and others. In recent years, new combinatorial techniques for the analysis of random planar maps, notably via random matrices and tree bijections, have revitalized the field. Some of these techniques were motivated from physics, in particular from conformal field theory and string theory.

There has been significant mathematical progress on the enumeration and scaling limits of random planar maps chosen uniformly from the set of all rooted planar maps with a given number of edges, beginning with the bijections of Cori–Vauquelin [10] and Schaeffer [59] and progressing to the

1

existence of Gromov–Hausdorff metric space limits established by Le Gall [43] and Miermont [45].

There has also emerged a large literature on planar maps that come equipped with additional structure, such as the instance of a model from statistical physics, e.g., a uniform spanning tree, or an Ising model configuration. These "decorated planar maps" are important in Euclidean 2D statistical physics. The reason is that it is often easier to compute "critical exponents" on planar maps than on deterministic lattices. Given the planar map exponents, one can apply the KPZ formula to *predict* the analogous Euclidean exponents.[1] In this paper, we consider random planar maps equipped with bipolar orientations.

1.2. *Bipolar and harmonic orientations.* A *bipolar (acyclic) orientation* of a graph G with specified source and sink (the "poles") is an acyclic orientation of its edges with no source or sink except at the specified poles. (A *source* (resp. *sink*) is a vertex with no incoming (resp. outgoing) edges.) For any graph G with adjacent source and sink, bipolar orientations are counted by the coefficient of x in the Tutte polynomial $T_G(x, y)$, which also equals the coefficient of y in $T_G(x, y)$; see [12] or the overview in [19]. In particular, the number of bipolar orientations does not depend on the choice of source and sink as long as they are adjacent. When the source and sink are adjacent, there are bipolar orientations precisely when the graph is biconnected, i.e., remains connected after the removal of any vertex [44]. If the source and sink are not adjacent, adjoining an edge between the source and sink does not affect the number of bipolar orientations, so bipolar orientations are counted by these Tutte coefficients in the augmented graph.

Let G be a finite connected planar map, with no self-loops but with multiple edges allowed, with a specified source and sink that are incident to the same face. It is convenient to embed G in the disk so that the source is at the bottom of the disk (and is denoted S, for south pole), the sink is at the top (and is denoted N, for north pole), and all other vertices are in the interior of the disk (see Figure 1). Within the disk there are two faces that are boundary faces, which can be called W (the west pole) and E (the east pole). Endowing G with a bipolar orientation is a way to endow it and its dual map G^* with a coherent notion of "north, south, east, and west": one may define the directed edges to point *north*, while their opposites point *south*.

---

[1]This idea was used by Duplantier to derive the so-called Brownian intersection exponents [15], whose values were subsequently verified mathematically by Lawler, Schramm, and Werner [39, 40, 41] in an early triumph of Schramm's SLE theory [60]. An overview with a long list of references can be found in [16].
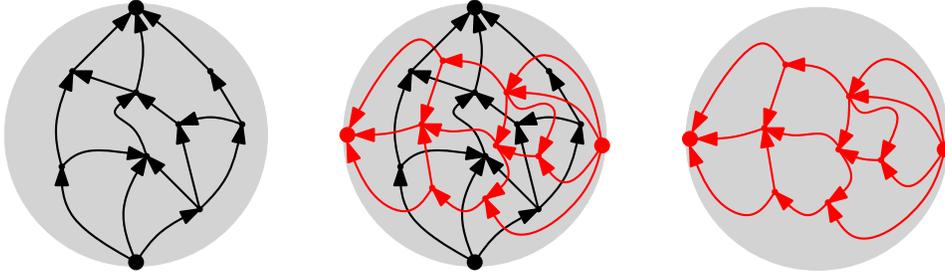
FIG 1. **Left:** *A planar map embedded in a disk with two boundary vertices, with a north-going bipolar orientation.* **Right:** *The dual bipolar-oriented planar map, which has two boundary dual vertices on the disk.* **Middle:** *Primal and dual bipolar-oriented maps together. The dual orientations are obtained from the primal orientations by rotating the arrows left.*

Each primal edge has a face to its *west* (left when facing north) and its *east* (right), and dual edges are oriented in the westward direction (Figure 1).

Given an orientation of a finite connected planar map G, its dual orientation of G^* is obtained by rotating directed edges counterclockwise. If an orientation has a sink or source at an interior vertex, its dual has a cycle around that vertex. Suppose an orientation has a cycle but has no source or sink at interior vertices. If this cycle surrounds more than one face, then one can find another cycle that surrounds fewer faces, so there is a cycle surrounding just one face, and the dual orientation has either a source or sink at that (interior) face. Thus an orientation of G is bipolar acyclic precisely when its dual orientation of G^* is bipolar acyclic. The east and west poles of G^* are the source and sink respectively of the dual orientation (see Figure 1).

One way to construct bipolar orientations is via electrical networks. Suppose every edge of G represents a conductor with some generic positive conductance, the south pole is at 0 volts, and the north pole is at 1 volt. The voltages are harmonic except at the boundary vertices, and for generic conductances, provided every vertex is part of a simple path connecting the two poles, the interior voltages are all distinct. The *harmonic orientation* orients each edge towards its higher-voltage endpoint. The harmonic orientation is clearly acyclic, and by harmonicity, there are no sources or sinks at interior vertices. In fact, for any planar graph with source and sink incident to the same face, *any* bipolar orientation is the harmonic orientation for some suitable choice of conductances on the edges [1, Thm. 1], so for this class of graphs, bipolar orientations are equivalent to harmonic orientations.

Suppose that a bipolar-oriented planar map G has an interior vertex in-

cident to at least four edges, which in cyclic order are oriented outwards, inwards, outwards, inwards. By the source-free sink-free acyclic property, these edges could be extended to oriented paths which reach the boundary, and by planarity and the acyclic property, the paths would terminate at four distinct boundary vertices. Since (in this paper) we are assuming that there are only two boundary vertices, no such interior vertices exist. Thus at any interior vertex, its incident edges in cyclic order consist of a single group of north-going edges followed by a single group of south-going edges, and dually, at each interior face the edges in cyclic order consist of a single group of clockwise edges followed by a single group of counterclockwise edges.

In particular, each vertex (other than the north pole) has a unique "west-most north-going edge," which is its NW edge. The *NW tree* is the directed tree which maps each vertex (other than the north pole) to its NW edge, and maps each edge to the vertex to its north. Geometrically, the NW tree can be drawn so that each NW edge is entirely in the NW tree, and for each other edge, a segment containing the north endpoint of the edge is in the NW tree (see Figure 2). We define southwest, southeast, and northeast trees similarly.

We will exhibit (see Theorems 2.1 and 2.2) a bijection between bipolar-oriented planar maps (with given face-degree distribution) and certain types of random walks in the nonnegative quadrant $\mathbb{Z}_{\geq 0}^2$. This bijection leads to exact enumerative formulae as well as local information about the maps such as degree distributions. For previous enumerative work on this model, including bijections between bipolar-oriented planar maps and other objects, see e.g. [19, 7, 6, 18].

1.3. *SLE and LQG.* After the bijections our second main result is the identification of the scaling limit of the bipolar-oriented map with a *Liouville quantum gravity* (LQG) surface decorated by a *Schramm-Loewner evolution* (SLE) curve, see Theorem 4.1.

We will make use of the fact proved in [14, 49, 21] that an SLE-decorated LQG surface can be equivalently defined as a mating of a correlated pair of continuum random trees (a so-called *peanosphere*; see Section 4.2) where the correlation magnitude is determined by parameters that appear in the definition of LQG and SLE (namely γ and κ').

The scaling limit result can thus be formulated as the statement that a certain pair of discrete random trees determined by the bipolar orientation (namely the *northwest* and *southeast* trees, see Section 1.2) has, as a scaling limit, a certain correlated pair of continuum random trees. Although LQG and SLE play a major role in our motivation and intuition (see Section 4.2),

we stress that no prior knowledge about these objects is necessary to understand either the main scaling limit result in the current paper or the combinatorial bijections behind its proof (Sections 2 and 3).

Before we move on to the combinatorics, let us highlight another point about the SLE connection. There are several special values of the parameters κ and $\kappa' = 16/\kappa$ that are related to discrete statistical physics models. (SLE$_\kappa$ with $0 < \kappa \leq 4$ and SLE$_{16/\kappa}$ are closely related [72, 13, 50, 55], which is known as SLE-duality.) These special $\{\kappa, \kappa'\}$ pairs include $\{2, 8\}$ (for loop-erased random walk and the uniform spanning tree) [42], $\{8/3, 6\}$ (for percolation and Brownian motion) [68, 38], $\{3, 16/3\}$ (for the Ising and FK-Ising model) [69, 9], and $\{4, 4\}$ (for the Gaussian free field contours) [61, 62]. The relationships between these special $\{\kappa, \kappa'\}$ values and the corresponding discrete models were all discovered or conjectured within a couple of years of Schramm's introduction of SLE, building on earlier arguments from the physics literature. We note that all of these relationships have random planar map analogs, and that they all correspond to $\{\kappa, \kappa'\} \subset [2, 8]$. This range is significant because the so-called *conformal loop ensembles* CLE$_\kappa$ [63, 66] are only defined for $\kappa \in (8/3, 8]$, and the discrete models mentioned above are all related to random collections of loops in some way, and hence have either κ or κ' in the range $(8/3, 8]$. Furthermore, it has long been known that ordinary SLE$_\kappa$ does not have time reversal symmetry when $\kappa > 8$ [58] (see [55] for the law of the time-reversal of such an SLE$_\kappa$ process), and it was thus widely assumed that discrete statistical physics systems would not converge to SLE$_\kappa$ for $\kappa > 8$ [8].

In this paper the relevant $\{\kappa, \kappa'\}$ pair is $\{4/3, 12\}$. This special pair is interesting in part because it lies outside the range $[2, 8]$. It has been proposed, based on heuristic arguments and simulations, that "activity-weighted" spanning trees should have SLE scaling limits with κ anywhere in the range $[4/3, 4)$ and κ' anywhere in the range $(4, 12]$ [36]. In more recent work, subsequent to our work on bipolar orientations, using a generalization of the inventory accumulation model in [65], the activity-weighted spanning trees on planar maps were shown to converge to SLE-decorated LQG in the peanosphere topology for this range of κ, κ' [35].

We will further observe that if one modifies the bipolar orientation model by a weighting that makes the faces more or less balanced (in terms of their number of clockwise and counterclockwise oriented boundary edges), one can obtain any $\kappa \in (0, 2)$ and any $\kappa' \in (8, \infty)$. In a companion to the current paper [37], we discuss a different generalization of bipolar orientations that we conjecture gives SLE for $\kappa \in [12 - 8\sqrt{2}, 4)$ and $\kappa' \in (4, 12 + 8\sqrt{2}]$.

In this article we consider an opposite pair of trees (NW-tree and SE-

tree). It is also possible to consider convergence of all four trees (NW, SE, NE, and SW) simultaneously: this is done in the recent article [34].

1.4. *Outline.*   In Sections 2 and 3 we establish our combinatorial results and describe the scaling limits of the NW and SE trees in terms of a certain two-dimensional Brownian excursion. In Section 4 we explain how this implies that the uniformly random bipolar-oriented map with n edges, and fixed face-degree distribution, decorated by its NW tree, converges in law as $n \to \infty$ to a $\sqrt{4/3}$-Liouville quantum gravity sphere decorated by space-filling SLE_{12} from ∞ to ∞. This means that, following the curve which winds around the NW tree, the distances to the N and S poles scale to an appropriately correlated pair of Brownian excursions. We also prove a corresponding *universality* result: the above scaling limit holds for essentially any distribution on face degrees (or, dually, vertex degrees) of the random map.

2. Bipolar-oriented maps and lattice paths.

2.1. *From bipolar maps to lattice paths.*   For the bipolar-oriented planar map in Figure 1, Figure 2 illustrates its *NW tree* (in red), *SE tree* (in blue), and the *interface path* (in green) which winds between them from the south pole to the north pole. The interface path has two types of steps:

1. Steps that traverse an edge (between red and blue sides).
2. Steps that traverse an interior face from its maximum to its minimum. Face steps can be subcategorized according to the number of edges on the west and east sides of the face, where the maximum and minimum vertex of a face separate its west from its east. If a face has $i + 1$ edges on its west and $j + 1$ edges on its east, we say that it is of type (i, j).

Observe that each face step has edge steps immediately before and after it.

Let E be the set of edges of the planar map, which we order $e_0, \ldots, e_{|E|-1}$ according to the green path going from the south pole S to the north pole
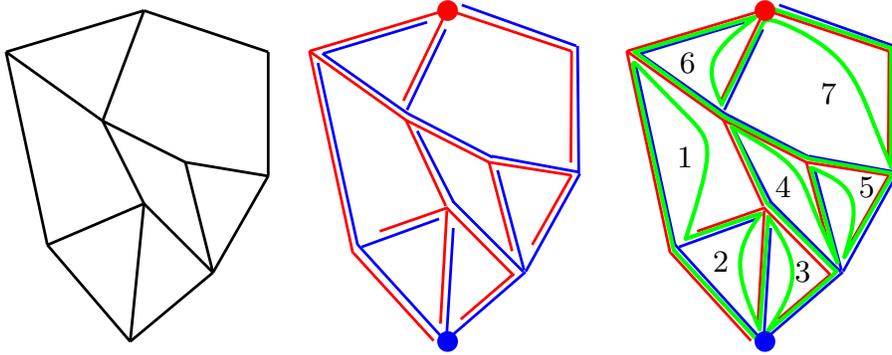
FIG 2. **Left:** *A map with a bipolar orientation, embedded so each edge is oriented "upward" (i.e., in the direction along which the vertical coordinate increases).* **Middle:** *Set of oriented edges can be understood as a tree, the northwest tree, where the parent of each edge is the leftmost upward oriented edge it can merge into. If we reverse the orientations of all edges, we can define an analogous tree (blue) and embed both trees (using the British convention of driving on the left side) so that they don't cross each other.* **Right:** *We then add a green path tracing the interface between the two trees. Each edge of the interface moves along an edge of the map or across a face of the map. For illustration purposes, faces are numbered by the order they are traversed by the green path, but it is the traversals of the edges of the green path that correspond to steps of the lattice path.*

N. For each edge e_t, let X_t be distance in the blue tree from the blue root (S) to the lower endpoint of e_t, and let Y_t be the distance in the red tree from the red root (N) to the upper endpoint of e_t. Suppose the west outer face has $m + 1$ edges and the east outer face has $n + 1$ edges. Then the sequence $\{(X_t, Y_t)\}_{0 \leq t \leq |E|-1}$ defines a walk or lattice path that starts at $(0, m)$ when $t = 0$ and ends at $(n, 0)$ when $t = |E| - 1$, and which remains in the nonnegative quadrant. If there is no face step between e_t and e_{t+1}, then the walk's increment $(X_{t+1}, Y_{t+1}) - (X_t, Y_t)$ is $(1, -1)$. Otherwise there is exactly one face step between e_t and e_{t+1}; if that face has $i + 1$ edges on its west and $j + 1$ edges on its east, then the walk's increment is $(-i, j)$, see Figure 3.

For the example in Figure 2, the walk starts at $(0, 2)$ and ends at $(3, 0)$.

2.2. *From lattice paths to bipolar maps.* The above construction can be reversed, constructing a bipolar-oriented planar map from a lattice path of the above type.

We construct the bipolar-oriented planar map by sewing edges and oriented polygons according to the sequence of steps of the path. Let $m_{i,j}$ denote a step of $(-i, j)$ with $i, j \geq 0$, and m_e denote a step of $(1, -1)$.

It is convenient to extend the bijection, so that it can be applied to any
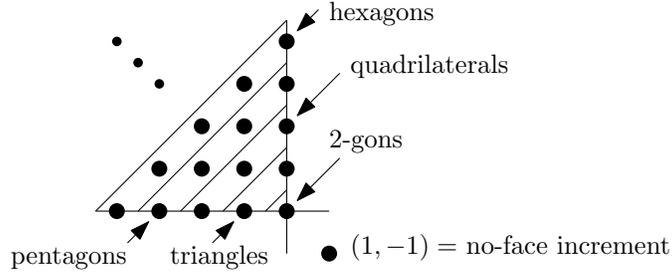
FIG 3. *Lattice path increments.*

sequence of these steps, not just those corresponding to walks remaining in the quadrant. These steps give sewing instructions to augment the current "marked bipolar map", which will be a slightly more general object.

A marked bipolar map is a bipolar-oriented planar map together with a "start vertex" on its western boundary which is not at the top, and an "active vertex" on its eastern boundary which is not at the bottom, such that the start vertex and every vertex below it on the western boundary has at most one downward edge, and the active vertex and every vertex above it on the eastern boundary has at most one upward edge. We think of the edges on the western boundary below the start vertex and on the eastern boundary above the active vertex as being "missing" from the marked bipolar map: they are boundaries of open faces that are part of the map, but are not themselves in the map.
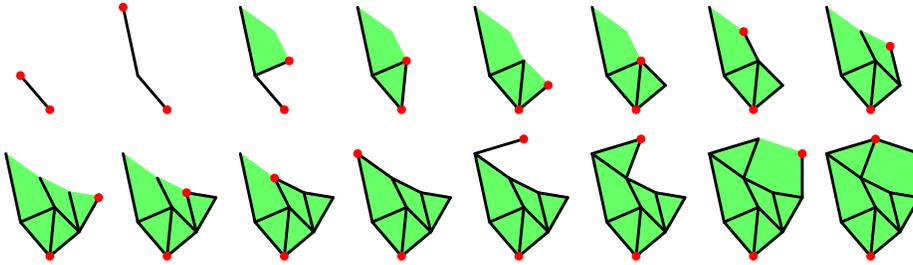
FIG 4. *The process of sewing oriented polygons and edges to obtain a bipolar-oriented planar map. The intermediate structures are marked bipolar-oriented planar maps, which may have some edges missing on the boundaries. The sequence of steps is:* $m_e, m_{0,2}, m_{1,0}, m_{0,1}, m_e, m_e, m_{1,1}, m_{0,1}, m_e, m_e, m_e, m_e, m_{1,0}, m_{2,1}, m_e.$

Initially the marked bipolar map consists of an oriented edge whose lower endpoint is the start vertex and whose upper endpoint is the active vertex.

Each m_e and $m_{i,j}$ move adds exactly one edge to the marked bipolar map. The $m_{i,j}$ moves also add an open face (and then adds in the southeastern edge)..

The m_e moves will sew an edge to the current marked bipolar map upwards from the active vertex and move the active vertex to the upper endpoint of the new edge. If the eastern boundary had a vertex above the active vertex, the new edge gets sewn to the southernmost missing edge on the eastern boundary, and otherwise there is a new vertex which becomes the current top vertex.

The $m_{i,j}$ moves will sew an open face with $i+1$ edges on its west and $j+1$ edges on its east, sewing the north of the face to the active vertex and the west of the face to the eastern boundary of the marked bipolar map, and then sew an edge to the southernmost east edge of the new face; the new active vertex is the upper vertex of this edge. We can think of $m_{i,j}$ as being composed of two submoves, a move $f_{i,j}$ which sews the open polygon to the structure, with the top of the polygon at the old active vertex, and with the new active vertex at the bottom of the polygon, followed by a regular m_e move. If there are fewer than $i+1$ edges below the (old) active vertex, then the new face gets sewn to as many of them as there are, the start vertex is no longer at the bottom, and the remaining western edges of the face are missing from the map. As seen in the proof of Theorem 2.2 below, this happens when the walk goes out of the positive quadrant; these western edges will remain missing for any subsequent steps.

The final marked bipolar map is considered a (unmarked) bipolar-oriented planar map if the start vertex is at the south and the active vertex is at the north, or equivalently, if there are no missing edges.

THEOREM 2.1.   *The above mapping from sequences of moves from $\{m_e\} \cup \{m_{i,j} : i, j \geq 0\}$ to marked bipolar maps is a bijection.*

PROOF. Consider a marked bipolar map obtained from a sequence of moves. The number of edges present in the structure determines the length of the sequence. If that length is positive, then the easternmost downward edge from the active vertex was the last edge adjoined to the structure. If this edge is the southernmost edge on the eastern boundary of a face, then the last move was one of the $m_{i,j}$'s, and otherwise it was m_e. Since the last move and preceding structure can be recovered, the mapping is an injection.

Starting from an arbitrary marked bipolar map, we can inductively define a sequence of moves as above by considering the easternmost downward edge from the active vertex. This sequence of moves yields the original marked bipolar map, so the mapping is a surjection.   □

Next we restrict this bijection to sequences of moves which give valid bipolar-oriented planar maps. A sequence of moves can of course be encoded as a path.

THEOREM 2.2.   *The above mapping gives a bijection from length-$(\ell - 1)$ paths from $(0, m)$ to $(n, 0)$ in the nonnegative quadrant having increments $(1, -1)$ and $(-i, j)$ with $i, j \geq 0$, to bipolar-oriented planar maps with ℓ total edges and $m+1$ and $n+1$ edges on the west and east boundaries respectively. A step of $(-i, j)$ in the walk corresponds to a face with degree $i + j + 2$ in the planar map.*

Note that for triangulations, the relevant increments are $(1, -1), (-1, 0)$ and $(0, 1)$. In this case, for a path of length ℓ, the number of steps of each type is determined (and equal to $\ell/3 + O(1)$).

PROOF. When we make a walk $(X_t, Y_t)_{t \geq 0}$ in $\mathbb{Z}^2$ started from (X_0, Y_0) using these moves, not necessarily confined to the quadrant, by induction

$$X_t - X_0 = -1 + (\# \text{ non-missing edges on the eastern boundary})$$
$$- (\# \text{ missing edges on the western boundary})$$

and

$$Y_t - Y_0 = 1 + (\# \text{ missing edges on the eastern boundary})$$
$$- (\# \text{ non-missing edges on the western boundary}) .$$

When the walk is started at $(0, m)$, the start vertex remains at the south pole precisely when the first coordinate always remains nonnegative. In this case, there are no missing edges on the western boundary, so the final number of non-missing edges on the eastern boundary is $n + 1$.

Suppose that we reverse the sequence of moves, and replace each $m_{i,j}$ with $m_{j,i}$, to obtain a new sequence. Write each $m_{i,j}$ as the face move $f_{i,j}$ followed by m_e. Recall that the initial structure was an edge; we may instead view the initial structure as a vertex followed by an m_e move. Written in this way, if the old sequence is $m_e^{k_0+1} f_{i_1,j_1} m_e^{k_1+1} f_{i_2,j_2} \cdots m_e^{k_q+1}$, the new sequence is $m_e^{k_q+1} \cdots f_{j_2,i_2} m_e^{k_1+1} f_{j_1,i_1} m_e^{k_0+1}$. We then see that the structure obtained from the new sequence is the same as the structure obtained from the old sequence but rotated by 180°, and with the roles of start and active vertices reversed.

Using this reversal symmetry with our previous observation, it follows that the active vertex is at the north pole precisely when the second coordinate

achieves its minimum on the last step (it may also achieve its minimum earlier), and the number of (non-missing) edges on the western boundary is $m + 1$.   □

If we wish to restrict the face degrees, the bijection continues to hold simply by restricting the set of allowed steps of the paths.

We can use the bijection to prove the following result:

THEOREM 2.3.   *Any finite bipolar-oriented planar map which has no self-loops or pairs of vertices connected by multiple edges has a straight-line planar embedding such that edges are oriented upwards, i.e., in the direction of increasing y-coordinate, as in Figure 2.*

PROOF. If the bipolar-oriented planar map has a face with more than 3 sides, then let $v_1, \ldots, v_4$ denote four of its vertices in cyclic order. The map could contain the edges (v_1, v_3) or (v_2, v_4), embedded outside the face, but it cannot contain both of them without violating planarity. We may adjoin an edge which the graph does not already contain, embed it within the face, and then orient it so that the augmented planar map is bipolar-oriented. By repeating this process, we see that we may assume that the map is a triangulation.

Given a bipolar-oriented triangulation without multiple edges between vertices, we can convert it to a walk using the bijection, and then convert it back to a bipolar triangulation again using the bijection. When converting the walk back to a triangulation, we do so while maintaining the following geometric property: We require that every edge, missing or non-missing, be embedded as a straight line oriented upwards. We also require that every pair of vertices on the right boundary of the closure of the structure have a "line-of-sight" to each other, unless the structure contains an edge (missing or non-missing) connecting them. By "having a line-of-sight", we mean that the open line segment connecting the vertices is disjoint from the closure of the structure.

It's trivial to make the initial structure satisfy the geometric property. Edge moves trivially maintain the geometric property. Since the graph does not contain multiple edges connecting vertices, the move $m_{1,0}$ (adjoining a leftward triangle) connects two vertices that are within line-of-site, so it also maintains the geometric property. The move $m_{0,1}$ adjoins a rightward triangle and necessarily makes the right boundary non-concave. However, for any pair of vertices on the right boundary that are within line-of-sight of each other, we may place the new vertex of the triangle sufficiently close to its left edge that the line-of-sight is not obstructed, and since there are

only finitely many pairs of vertices on the right boundary, we may embed the new triangle so that the geometric property is maintained.

By induction the final structure satisfies the geometric property, so it is a straight-line embedding with edges oriented upwards. □

2.3. *Path scaling limit.* What happens if we consider a random bipolar-oriented planar map such as the one in Figure 2, where we fix the left boundary length (3 in Figure 2), the right boundary length (4 in Figure 2), and the total number ℓ of edges (16 in Figure 2)? We consider the limiting case where the boundary lengths are fixed and $\ell \to \infty$. What can one say about the limiting joint law of the pair of trees in Figure 2 in this situation?

In light of Theorem 2.2, understanding this limiting law amounts to understanding the limiting law of its associated lattice path. For example, if the map is required to be a triangulation, we should consider a random walk of length $\ell - 1$ with steps $(1, -1), (-1, 0)$ and $(0, 1)$, each chosen with probability $1/3$ (by the comment after the statement of Theorem 2.2) conditioned to start and end at certain fixed values, and to stay in the nonnegative quadrant.

It is reasonable to expect that if a random walk on $\mathbb{Z}^2$ converges to Brownian motion with some non-degenerate diffusion matrix, then the same random walk conditioned to stay in a quadrant (starting and ending at fixed locations when the number of steps gets large) should scale to a form of the Brownian excursion, i.e., a Brownian bridge constrained to stay in the same quadrant (starting and ending at 0). The recent work [17, Theorem 4] contains a precise theorem of this form, and Proposition 2.4 below is a special case of this theorem. (The original theorem is for walks with a diagonal covariance matrix, but supported on a generic lattice, which implies Proposition 2.4 after applying a linear transformation to the lattice.)

Recall that the period of a random walk on $\mathbb{Z}^2$ is the smallest integer $p \geq 1$ such that the random walk has a positive probability to return to zero after kp steps for all sufficiently large integers $k > 0$.

PROPOSITION 2.4.   *Let ν be a probability measure supported on $\mathbb{Z}^2$ with expectation zero and moments of all orders. Let $p \geq 1$ denote the period of the random walk on $\mathbb{Z}^2$ with step distribution ν. Suppose that for given $z_{start}, z_{end} \in \mathbb{Z}_{\geq 0}^2$, for some ℓ there is a positive probability path in $\mathbb{Z}_{\geq 0}^2$ from z_{start} to z_{end} with ℓ steps from ν. Suppose further that for any $R > 0$ there is a point $z \in \mathbb{Z}_{\geq 0}^2$ that is distance at least R from the boundary of the quadrant, such that there is a path from z_{start} to z to z_{end} with steps from ν that remains in the quadrant $\mathbb{Z}_{\geq 0}^2$. For sufficiently large n with $n \equiv \ell \bmod p$, consider a random walk $z_{start} = S_0, S_1, \ldots, S_n = z_{end}$ from z_{start} to z_{end} with*

increments chosen from ν, conditioned to remain in the quadrant $\mathbb{Z}^2_{\geq 0}$. Then the law of $S_{\lfloor nt \rfloor}/\sqrt{n}$ converges weakly w.r.t. the L^∞ norm on $[0,1]$ to that of a Brownian excursion (with diffusion matrix given by the second moments of ν) into the nonnegative quadrant, starting and ending at the origin, with unit time length.

In fact in this statement we do not need ν to have moments of all orders; it suffices that $|\cdot|^\alpha$ has ν-finite expectation, for a positive constant α defined in [17]. The constant α depends on the angle of the cone $L(\mathbb{R}^2_{\geq 0})$, where $L : \mathbb{R}^2 \to \mathbb{R}^2$ is a linear map for which $L(S_n)$ scales to a constant multiple of standard two-dimensional Brownian motion. In the setting of Theorems 2.5 and 2.6 below, L can be the map that rescales the $(1, -1)$ direction by $1/\sqrt{3}$ and fixes the $(1,1)$ direction. In this case, the cone angle is $\pi/3$ and $\alpha = 3$.

The correlated Brownian excursion (X, Y) in $\mathbb{R}^2_{\geq 0}$ referred to in the statement of Proposition 2.4 is characterized by the Gibbs resampling property, which states that the following is true. For any $0 < s < t < 1$, the conditional law of (X, Y) in $[s, t]$ given its values in $[0, s]$ and $[t, 1]$ is that of a correlated Brownian motion of time length $t - s$ starting from $(X(s), Y(s))$ and finishing at $(X(t), Y(t))$ conditioned on the positive probability event that it stays in $\mathbb{R}^2_{\geq 0}$. The existence of this process follows from the results of [67]; see also [20].

Now let us return to the study of random bipolar-oriented planar triangulations. By Theorem 2.2 these correspond to paths in the nonnegative quadrant from the y-axis to the x-axis which have increments of $(1, -1)$ and $(0, 1)$ and $(-1, 0)$. Fix the boundary lengths $m + 1$ and $n + 1$, that is, fix the start $(0, m)$ and end $(n, 0)$ of the walk, and let the length ℓ get large. Note that if ν is the uniform measure on the three values $(1, -1)$ and $(0, 1)$ and $(-1, 0)$, then the ν-expectation of an increment (X, Y) of the (unconstrained) walk is $(0, 0)$. Furthermore, (in the unconstrained walk) the variance of $X - Y$ is 2 while the variance of $X + Y$ is $2/3$, and the covariance of $X - Y$ and $X + Y$ is zero by symmetry. Thus the variance in the $(1, -1)$ direction is 3 times the variance in the $(1, 1)$ direction. The scaling limit of the random walk will thus be a Brownian motion with the corresponding covariance structure. We can summarize this information as follows:

THEOREM 2.5.   *Consider a uniformly random bipolar-oriented triangulation, sketched in the manner of Figure 2, with fixed boundary lengths $m+1$ and $n+1$ and with the total number of edges given by ℓ. Let $S_0, S_1, \ldots, S_{\ell-1}$ be the corresponding lattice walk. Then $S_{\lfloor \ell t \rfloor}/\sqrt{\ell}$ converges in law (weakly w.r.t. the L^∞ norm on $[0,1]$), as $\ell \to \infty$ with $\ell \equiv -m - n + 1 \bmod 3$, to the Brownian excursion in the nonnegative quadrant starting and ending at the*

origin, with covariance matrix $\begin{pmatrix} 2/3 & -1/3 \\ -1/3 & 2/3 \end{pmatrix}$. *(This is the covariance matrix such that if the Brownian motion were unconstrained, the difference and sum of the two coordinates at time 1 would be independent with respective variances 2 and $2/3$.)*

In particular, Theorem 2.5 holds when the lattice path starts and ends at the origin, so that the left and right sides of the planar map each have length 1. In this case, the two sides can be glued together and treated as a single edge in the sphere, and Theorem 2.5 can be understood as a statement about bipolar maps on the sphere with a distinguished south to north pole edge.

Next we consider more general bipolar-oriented planar maps. Suppose we allow not just triangles, but other face sizes. Suppose that for nonnegative weights $a_2, a_3, \ldots$, we weight a bipolar-oriented planar map by $\prod_{k=2}^{\infty} a_k^{n_k}$ where n_k is the number of faces with k edges, and we use the convention $0^0 = 1$. (Taking $a_k = 0$ means that faces with k edges are forbidden.) For maps with a given number of edges, this product is finite. Then we pick a bipolar-oriented planar map with ℓ edges with probability proportional to its weight; the normalizing constant is finite, so this defines a probability measure if at least one bipolar map has positive weight.

To ensure that such bipolar maps exist, there is a congruence-type condition involving the number of edges ℓ and the set of face sizes k with positive weight a_k. We also use an analytic condition on the set of weights a_k to ensure that random bipolar maps are not concentrated on maps dominated by small numbers of large faces. When both these conditions are met, we obtain the limiting behavior as $\ell \to \infty$.

THEOREM 2.6.   *Suppose that nonnegative face weights $a_2, a_3, \ldots$ are given, and $a_k > 0$ for at least one $k \geq 3$. Let*

$$(1) \qquad b = \gcd\left(\{k \geq 1 : a_{2k} > 0\} \cup \{2k+1 \geq 3 : a_{2k+1} > 0\}\right).$$

Consider a bipolar-oriented planar map with fixed boundary lengths $m+1$ and $n+1$ and with the total number of edges given by ℓ, chosen with probability proportional to the product of the face weights. If $m + n$ is odd and all face sizes are even, or if

$$(2) \qquad\qquad 2 \times (\ell - 1) \equiv m + n \bmod b,$$

does not hold, then there are no such maps; otherwise, for ℓ large enough there are such maps. Let $S_0, S_1, \ldots, S_{\ell-1}$ be the corresponding lattice walk.

Suppose $\sum_k a_k z^k$ has a positive radius of convergence R, and

$$(3) \qquad 1 \le \sum_{k=2}^{\infty} \frac{(k-1)(k-2)}{2} a_k R^k .$$

Then for some finite λ with $0 < \lambda \le R$

$$(4) \qquad 1 = \sum_{k=2}^{\infty} \frac{(k-1)(k-2)}{2} a_k \lambda^k .$$

Suppose further $\lambda < R$, or $\lambda = R$ but also $\sum_k k^4 a_k R^k < \infty$. Then as $\ell \to \infty$ while satisfying (2), the scaled walk $S_{\lfloor \ell t \rfloor}/\sqrt{\ell}$ converges in law (weakly w.r.t. the L^∞ norm on $[0,1]$), to the Brownian excursion in the nonnegative quadrant starting and ending at the origin, with covariance matrix that is a scalar multiple of $\begin{pmatrix} 2/3 & -1/3 \\ -1/3 & 2/3 \end{pmatrix}$.

Furthermore, the walk is locally approximately i.i.d. in the following sense: fix $J > 0$ and suppose that for some $\ell > J$ we sample M uniformly from $\{1, \dots, \ell - J\}$, and consider the sequence given by the first J moves after the Mth step; then as $\ell \to \infty$ the law of this sequence converges in total variation to that of an i.i.d. sequence, in which move $m_{i,j}$ occurs with probability $a_{i+j+2} \lambda^{i+j}/C$ and move m_e occurs with probability λ^{-2}/C, and C is a normalizing constant.

REMARK 2.7. The constraint (3) is to ensure that (4) can be satisfied, which will imply that the lattice walk has a limiting step distribution that has zero drift. The constraint that $\lambda < R$, or $\lambda = R$ but also $\sum_k k^4 a_k R^k < \infty$ implies that the limiting step distribution has finite third moment. When the weights $a_2, a_3, \dots$ do not satisfy these constraints, the random walk excursion does not in general converge to a Brownian motion excursion. Can one characterize bipolar-oriented planar maps in these cases? Can the inequality $\sum_k k^4 a_k \lambda^k < \infty$ be replaced with $\sum_k k^3 a_k \lambda^k < \infty$ (finite second moment for the step distribution)?

REMARK 2.8. Theorem 2.6 applies to triangulations (giving Theorem 2.5 except for the scalar multiple in the covariance matrix), quadrangulations, or k-angulations for any fixed k, or more generally when one allows only a finite set of face sizes. The bound (3) is trivially satisfied in these cases since the radius of convergence is $R = \infty$.

REMARK 2.9. In the case where $1 = a_2 = a_3 = \cdots$, i.e., the uniform distribution on bipolar-oriented planar maps, the radius of convergence is

$R = 1$, and $\lambda = 1/2$, so Theorem 2.6 applies. The step distribution ν of the walk is

$$\nu\{(-i,j)\} = \begin{cases} 2^{-i-j-3} & i,j \geq 0 \ \text{ or } \ i = j = -1 \\ 0 & \text{otherwise.} \end{cases}$$

In this case it is also possible to derive the distribution ν for uniformly random bipolar-oriented planar maps using a different bijection, one to noncrossing triples of lattice paths [19].

REMARK 2.10.   Under the hypotheses of Theorem 2.6, with p_k defined as in (6) below, dividing (5) by C shows that in a large random map a randomly chosen face has degree k with limiting probability

$$\mathbb{P}(\text{face has degree } k) \to \frac{(k-1)p_k}{1 - p_0}.$$

PROOF OF THEOREM 2.6. Since the right-hand side of (4) increases monotonically from 0 and is continuous on $[0, R)$, (3) implies the existence of a solution $\lambda \in (0, R]$ to (4). Since $a_k > 0$ for some $k \geq 3$, $\lambda < \infty$.

Next let $a_0 = 1$ and define

$$(5) \qquad\qquad C = \frac{a_0}{\lambda^2} + \sum_{k=2}^{\infty} (k-1)a_k \lambda^{k-2},$$

which by our hypotheses is finite, and define

$$(6) \qquad\qquad p_k = \frac{a_k \lambda^{k-2}}{C}.$$

Then (dividing (5) by C) the p_k's define a random walk (X_t, Y_t) in $\mathbb{Z}^2$, which assigns probabilities p_0 and p_{i+j-2} to steps m_e and $m_{i,j}$ respectively (recall that there are $k - 1$ possible steps of type $m_{i,j}$ where $i + j = k - 2$, corresponding to a k-gon).

If we pick a random walk of length $\ell - 1$ from z_{start} to z_{end} weighted by the a_k's, it has precisely the same distribution as it would have if we weighted it by the p_k's instead, because the total exponent of λ for a walk from z_{start} to z_{end} is $y_{\text{end}} - x_{\text{end}} - y_{\text{start}} + x_{\text{start}}$, and because the total exponent of C is $\ell - 1$. The advantage of working with the p_k's rather than the a_k's is that they define a random walk, which, as we verify next, has zero drift.

The drift of $X_t + Y_t$ is zero by symmetry. The drift of $X_t - Y_t$ is

$$(7) \qquad\qquad 2p_0 - \sum_{k \geq 2} (k-2)(k-1)p_k$$

which is zero by the definition of p_k and (4).

Next we determine the period of the walk in $\mathbb{Z}^2$. Consider the antidiagonal direction $Y_t - X_t$. A move of type m_e decreases this by 2, and a move of type $m_{i,j}$, corresponding to a k-gon with $k = i + j + 2$, increases it by $k - 2$. For even k, consider the special case of a move of type $m_{k/2-1,k/2-1}$. This type of move followed by $k/2 - 1$ moves of type m_e returns the walk to its start after $k/2$ total moves. For odd k, consider another special case: a move of type $m_{k-2,0}$ and a move of type $m_{0,k-2}$ followed by $k - 2$ moves of type m_e returns the walk to its start after k total moves. So we see that the period of the walk is no larger than b as defined in (1). If the period were smaller, then we could consider a minimal nonempty set of t moves for which $Y_t - X_t = Y_0 - X_0$ and $b \nmid t$. Such a minimal set would contain no k-gon moves for even k (since we could remove a k-gon move and $k/2 - 1$ type m_e moves to get a smaller set), and at most one k-gon move for any given odd k (since for odd k we can remove k-gon moves in pairs along with $k - 2$ type m_e moves to get a smaller set). Let $k_1, \ldots, k_r$ be these odd k's. There are $(k_1 + \cdots + k_r - 2r)/2$ m_e moves, for a total of $(k_1 + \cdots + k_r)/2$ moves. Then $2t = k_1 + \cdots + k_r$, and since $b \mid k_1, \ldots, b \mid k_r$, we have $b \mid 2t$. Since $r \geq 1$, $b \mid k_1$, so b is odd, and so in fact $b \mid t$. Hence both the walk (X_t, Y_t) and its projection $Y_t - X_t$ are periodic with period b.

For a face of size k, let $q(k) = k/2$ if k is even and $q(k) = k$ if k is odd. The period b is an integer linear combination of finitely many terms $q(k_1) < \cdots < q(k_s)$ where $a_{k_i} > 0$. We claim that any multiple of b which is at least $(s - 1)q(k_s)^2$ is a nonnegative-integer linear combination of $q(k_1), \ldots, q(k_s)$. To see this, let c be a multiple of b that is at least $(s-1)q(k_s)^2$. We may write $c = \sum_{i=1}^{s} \beta_i q(k_i)$ where $\beta_i \in \mathbb{Z}$; suppose that we choose the coefficients $\beta_1, \ldots, \beta_s$ to maximize the sum of the negative coefficients. If some coefficient β_i is negative, then there is another coefficient β_j for which $\beta_j q(k_j) \geq q(k_s)^2 > q(k_i)q(k_j)$, in which case we could decrease β_j by $q(k_i)$ and increase β_i by $q(k_j)$ to increase the sum of the negative coefficients. This completes the proof of the claim. Thus the period of the walk in $\mathbb{Z}^2$ (not confined to the quadrant) is b.

Suppose a walk in $\mathbb{Z}^2$ starts at $(0, m)$ and goes to $(n, 0)$ after $t = \ell - 1$ steps. Consider the walk's projection in the antidiagonal direction: $(Y_t - X_t) - (Y_0 - X_0) = -m - n$. If $m + n$ is even, then the projected walk can reach its destination after $(m + n)/2$ m_e moves, and since b is the period, it follows that $\ell - 1 \equiv (m + n)/2 \bmod b$. If $m + n$ is odd, then for the walk to have positive probability there must be some odd k with $a_k > 0$. The projected walk can reach its destination after an $m_{k-2,0}$ move and $(m + n + k - 2)/2$ m_e moves, and since b is the period of the walk (and b is a multiple of k, by

definition of b), $\ell - 1 \equiv (m + n + k)/2 \mod b$. In either case, the existence of such a walk implies $2(\ell - 1) \equiv m + n \mod b$.

If there are only even face sizes and $m + n$ is odd, there are no walks from $(0, m)$ to $(n, 0)$. Otherwise, whether $m + n$ is even or there is an odd face size, we can first choose face moves to change the $X_t + Y_t$ coordinate from m to n, and then follow them by some number of m_e moves to change the $Y_t - X_t$ coordinate to $-n$. We may then follow these moves by a path from $(n, 0)$ to itself with length given by any sufficiently large multiple of b. Thus, for any sufficiently large ℓ with $2(\ell - 1) \equiv m + n \mod b$, there is a walk within $\mathbb{Z}^2$ (not confined to the quadrant) from $(0, m)$ to $(n, 0)$.

Next pick a face size $k \geq 3$ for which $a_k > 0$. For $s \geq 0$, the above walk in $\mathbb{Z}^2$ from $(0, m)$ to $(n, 0)$ can be prepended with $(m_{0,k-2}^2 m_e^{k-2})^s$ and postpended with $(m_e^{k-2} m_{k-2,0}^2)^s$, and it will still go from $(0, m)$ to $(n, 0)$. For some sufficiently large s, the walk will not only remain in the quadrant but will also travel arbitrarily far from the boundary of the quadrant, which gives the paths required by Proposition 2.4.

The variances of $X - Y$ and $X + Y$ are respectively

$$(8) \qquad \mathrm{Var}[X - Y] = 4p_0 + \sum_{k \geq 2} (k - 2)^2 (k - 1) p_k,$$

and

$$(9) \quad \mathrm{Var}[X+Y] = \sum_{k \geq 2} p_k ((k-2)^2 + (k-4)^2 + \cdots + (-k+2)^2) = \sum_{k \geq 2} p_k \times 2 \binom{k}{3},$$

which are both positive and finite by our hypotheses. Using the zero-drift condition (7), we may combine (8) and (9) to obtain

$$\mathrm{Var}[X - Y] = \sum_{k \geq 2} (k-2)(k-1)k\, p_k = \sum_{k \geq 2} p_k\, 6 \binom{k}{3} = 3\, \mathrm{Var}[X + Y].$$

Then we apply Proposition 2.4. Since the ratio of variances is 3, we need the walk's step distribution to have a finite third moment (see the comments after Proposition 2.4). Since there are $|k - 1|$ steps of type p_k, the third moment of the step distribution is finite when

$$\sum_{k \geq 2} p_k k^4 = \frac{1}{C} \sum_{k \geq 2} a_k \lambda^{k-2} k^4 < \infty$$

which is implied by our hypotheses. Hence by Proposition 2.4 the scaling limit of the walk is a correlated Brownian excursion in the quadrant.

The local approximate i.i.d. nature of the walk follows from a standard entropy maximization argument (Cramer's theorem implies that *if* the steps were i.i.d. the probability that the empirical pattern density for length-J blocks of moves differs from its expectation by any fixed amount would decay exponentially; however under this i.i.d. law the probability that the walk stays in the quadrant and has the desired starting and ending points has a power law decay, which means that even conditioned on staying in the quadrant, the pattern density is sufficiently well concentrated in the $\ell \to \infty$ limit.) □

REMARK 2.11. If one relaxes the requirement that the probabilities assigned by the step distribution ν be the same for all increments corresponding to a given face size, one can find a ν such that the expectation is still $(0,0)$ and when (X,Y) is sampled from ν, the law is still symmetric w.r.t. reflection about the line $y = -x$ but the variance ratio $\mathrm{Var}[X-Y]/\mathrm{Var}[X+Y]$ assumes any value strictly between 1 and ∞. Indeed, one approaches one extreme by letting (X,Y) be (close to being) supported on the $y = -x$ antidiagonal, and the other extreme by letting (X,Y) be (close to being) supported on the x- and y-axes far from the origin (together with the point $(1,-1)$). The former corresponds to a preference for nearly balanced faces (in terms of the number of clockwise and counterclockwise oriented edges) while the latter corresponds to a preference for unbalanced faces.

REMARK 2.12. In each of the models treated above, it is natural to consider an "infinite-volume limit" in which lattice path increments indexed by $\mathbb{Z}$ are chosen i.i.d. from ν. The standard central limit theorem then implies that the walks have scaling limits given by a Brownian motion with the appropriate covariance matrix.

3. Bipolar-oriented triangulations.

3.1. *Enumeration.* The following corollary is an easy consequence of the bijection. The formula itself goes back to Tutte [71]; Bousquet-Melou gave another proof together with a discussion of the bipolar orientation interpretation [7, Prop. 5.3, eqn. (5.11) with $j = 2$].

COROLLARY 3.1. *The number of bipolar-oriented triangulations of the sphere with ℓ edges in which S and N are adjacent and marked is (with $\ell = 3n$)*

$$B_\ell = \frac{2\,(3n)!}{(n+2)!\,(n+1)!\,n!}$$

(and zero if ℓ is not a multiple of 3).

PROOF. In a triangulation $2E = 3F$ so the number of edges is a multiple of 3. Since S and N are adjacent, there is a unique embedding in the disk so that the west boundary has length 1 and the east boundary has length 2. The lattice walks as discussed there go from $(0,0)$ to $(1,0)$. It is convenient to concatenate the walk with a final $m_{1,0}$ step, so that the walks are from $(0,0)$ to $(0,0)$ of length ℓ and remain in the first quadrant; moreover the number of steps of each type must be equal. Applying a shear $\begin{pmatrix} 1 & 0 \\ 1 & 1 \end{pmatrix}$, the walks with steps $m_e, m_{0,1}, m_{1,0}$ become walks with steps $(1,0), (0,1), (-1,-1)$ which remain in the domain $y \geq x \geq 0$. Replacing these steps by $(1,0,0), (0,1,0), (0,0,1)$ respectively, this is the number of walks from $(0,0,0)$ to (n,n,n) with steps $(1,0,0), (0,1,0), (0,0,1)$ remaining in the domain $y \geq x \geq z$. These are the so-called 3D Catalan numbers, see A005789 in the OEIS. □

3.2. *Vertex degree.*   Using the bijection between paths and bipolar-oriented maps, we can easily get the distribution of vertex degrees of a large bipolar-oriented triangulation.

PROPOSITION 3.2.   *In a large bipolar-oriented planar triangulation with fixed boundary lengths $m+1$ and $n+1$, as the number of edges ℓ tends to ∞ with $\ell + m + n \equiv 1 \bmod 3$, the limiting in-degree and out-degree distributions of a random vertex are independent and geometrically distributed (starting at 1) with mean 3.*

PROOF. We examine the construction of bipolar-oriented planar maps when the steps give triangles. Any new vertex or new edge is adjoined to the marked bipolar map on its eastern boundary, which we also call the *frontier*.

A new vertex is created by an $m_{0,1}$ move, or an m_e move if there are currently no frontier vertices above the active vertex, and when a vertex is created it is the active vertex. Each subsequent move moves frontier vertices relative to the active vertex, so let us record their position with respect to the active vertex by integers, with positive integers recording the position below the active vertex and negative integers recording the position above it. See Figure 5.

The following facts are easily verified.

1. A vertex moves off the frontier exactly when it is at position 1 and an $m_{1,0}$ move takes place.
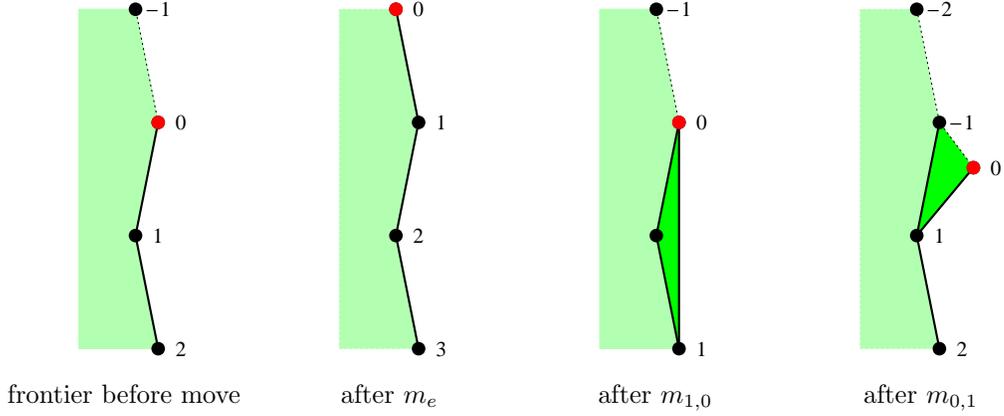
frontier before move   after m_e after $m_{1,0}$ after $m_{0,1}$

FIG 5. *Action of the three moves* $m_e, m_{1,0}, m_{0,1}$ *on the frontier. The vertex positions (relative to the active vertex) are shown.*

2. m_e moves increase the index of vertices by 1.
3. $m_{0,1}$ moves decrease the index of a vertex by 1 if it is non-positive, else leave it fixed.
4. $m_{1,0}$ moves decrease the index by 1 if it is ≥ 2, else leave it fixed (if the index is 1 it is moved off of the frontier).
5. Except for the start vertex of the initial structure, whenever a vertex is created, its in-degree is 1 and its out-degree is 0.
6. The in-degree of a vertex increases by 1 each time it visits position 0, the out-degree increases each time it visits position 1.

The transition diagram is summarized here:
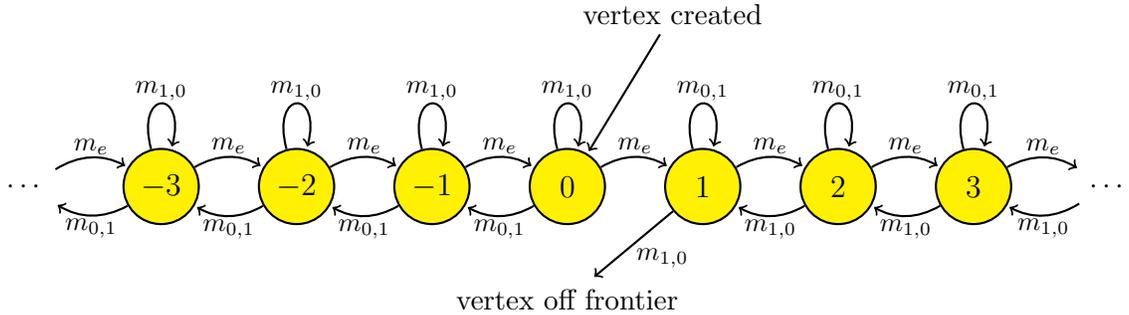
For the purposes of computing the final in-degree and out-degree of a ver-

tex, we can simply count the number of visits to 0 before its index becomes positive, and then count the number of visits to 1 before it is absorbed in the interior of the structure.

Since m and n are held fixed as $\ell \to \infty$, almost all vertices in the bipolar map are created by $m_{0,1}$ moves. By the local approximate i.i.d. property of the walk proved in Theorem 2.6, we see that the moves in the transition diagram above converge weakly to a Markov chain where each transition occurs with probability $1/3$.

The Markov chain starts at 0, and on each visit to 0 there is a $1/3$ chance of going to 1 and a $2/3$ chance of eventually returning to 0. On each visit to 1, there is a $1/3$ chance of exiting and a $2/3$ chance of eventually returning to 1. In the Markov chain, the number of visits to 0 and 1 are a pair of independent geometric random variables with minimum 1 and mean 3, which in view of fact 6 above, implies the proposition. $\qquad\square$

4. Scaling limit.

4.1. *Statement.*   In order to prove that random discrete objects converge to random continuous objects, one has to specify what that convergence means. Typically, one begins by describing a topological space that includes both the discrete objects and the continuous objects as elements.

As we discuss in Section 4.2 below, many kinds of discrete and continuum tree-decorated surfaces can be naturally encoded by pairs of interface functions, such as the (X_t, Y_t) process in this paper.

Let $C = C([0,1], \mathbb{R}^2)$ be the space of continuous functions from $[0,1]$ to $\mathbb{R}^2$ with the uniform metric (sup-norm metric). Let $\mathcal{C}$ be the corresponding weak topology on the set S_C of *probability measures* on C. One way to say that a sequence of random discrete tree-decorated surfaces converge to a random continuum tree-decorated surface is to say that the laws of the corresponding interface functions converge as elements of $(S_C, \mathcal{C})$. This property in fact defines a topology on the space of tree-decorated surfaces (with parameterized interface functions), called the peanosphere topology: We define in section 4.2 a map g that takes a (discrete or continuous) tree-decorated surface of the type we consider here to an element of C. The g^{-1} pullback of the sup-norm topology on C is the *peanosphere topology* on a space that includes both discrete and continuous tree-decorated surfaces. Theorem 4.1 below is a statement about convergence in law w.r.t. this topology. Note that (since $\mathcal{C}$ is a topology on measures) it is not necessary that g be defined for *every conceivable* tree-decorated surface, as long as it is defined for a.a. tree-decorated surfaces that arise in the random models we are considering.

At this point the reader may object: if Theorem 4.1 is in essence a statement about the scaling limits of random interface functions, it may seem

like an unnecessary bit of semantics to *interpret* it as a statement about the convergence of the random tree-decorated surfaces themselves (in the peanosphere topology). On the other hand, there are good mathematical reasons to consider this interpretation. This is because there are various other topologies (involving Gromov-Hausdorff metrics, conformal embeddings, etc.) w.r.t. which discrete tree-decorated surfaces have been *conjectured* to converge to their continuous counterparts, and it is often the case in this subject that once one has convergence in one topology, one can *extend* the convergence to other topologies without having to start from scratch (and some specific examples of results along these lines are cited below).

The proof of Theorem 4.1 is an easy computation upon application of the infinite-volume tree-mating theory introduced in [14], a derivation of the relationship between the SLE/LQG parameters and a certain variance ratio in [14, 21], and a finite volume elaboration in [49]. As mentioned above, we will explain this further in Section 4.2 just below.

THEOREM 4.1. *The scaling limit of the bipolar-oriented planar map with its interface curve, with fixed boundary lengths $m+1$ and $n+1$, and number of edges $\ell \to \infty$ (with a possible congruence restriction on ℓ, m, and n to ensure such maps exist), with respect to the peanosphere topology, is a $\sqrt{4/3}$-LQG sphere decorated by an independent* SLE$_{12}$ *curve.*

We remark that the peanosphere topology is neither coarser nor finer than other natural topologies, including in particular those that we discuss in the Section 4.2.

PROOF OF THEOREM 4.1. In Section 2.3 it was shown that the interface function for the bipolar-oriented random planar map converges as $\ell \to \infty$ to a Brownian excursion (X, Y) in the non-negative quadrant having covariance matrix (up to scale) $\begin{pmatrix} 2/3 & -1/3 \\ -1/3 & 2/3 \end{pmatrix}$, that is $X-Y$ and $X+Y$ are independent, and $\mathrm{Var}[X - Y] = 3\mathrm{Var}[X + Y]$.

The fact that the limit is a Brownian excursion implies, by [14, Theorem 1.13] and the finite volume variant in [49] and [21, Theorem 1.1], that the scaling limit in the peanosphere topology is a peanosphere, that is, a γ-LQG sphere decorated by an independent space-filling SLE$_{\kappa'}$, for a certain γ, κ'. The values γ, κ' are determined by the covariance structure of the limiting Brownian excursion. The ratio of variances $\mathrm{Var}[X - Y]/\mathrm{Var}[X + Y]$ takes the form

(10) $$(1 + \cos[4\pi/\kappa'])/(1 - \cos[4\pi/\kappa']).$$

This relation was established for $\kappa' \in (4, 8]$ in [14], and more generally for $\kappa' \in (4, \infty)$ in [21].[2] Setting it equal to 3 and solving we find $\kappa' = 12$. For this value of κ' we have $\gamma = \sqrt{16/\kappa'} = \sqrt{4/3}$.   □

REMARK 4.2.   If the covariance ratios vary as in Remark 2.11, then the κ' values varies between 8 and ∞. In other words, one may obtain any $\kappa' \in (8, \infty)$, and corresponding $\gamma = \sqrt{16/\kappa'}$, by introducing weightings that favor faces more or less balanced.

REMARK 4.3.   The infinite-volume variant described in Remark 2.12 corresponds to the mated pair of *infinite-diameter* trees first described in [14], which in turn corresponds to the so-called γ-quantum cone described in the next subsection.
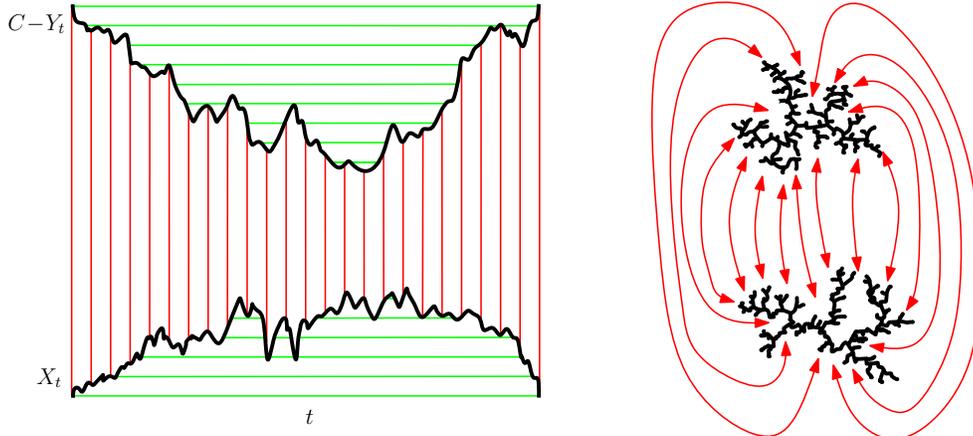

FIG 6.   *Gluing together a pair of CRTs to obtain a topological sphere. Illustration of the peanosphere construction. (This figure first appeared in [14].)*

4.2. *Peanosphere background.*   The purpose of this section is to give a brief description of how Liouville quantum gravity (LQG) surfaces [16] decorated by independent SLE processes can be viewed as matings of random trees which are related to Aldous' continuum random tree (CRT) [2, 3, 4].

---

[2]There is as yet no analogous construction corresponding to the limiting case $\kappa' = 4$, where (10) is zero so that $\text{Var}(X - Y) = 0$ and $X = Y$ a.s. It is not clear what such a construction would look like, given that space-filling $\text{SLE}_{\kappa'}$ has only been defined for $\kappa' > 4$, not for $\kappa' = 4$, and the peanosphere construction in Section 4.2 is trivial when the limiting Brownian excursion is supported on the diagonal $x = y$.

The results that underlie this perspective are established in [14, 49], building on prior results from [16, 64, 63, 50, 51, 52, 55].

Recall that if h is an instance of the Gaussian free field (GFF) on a planar domain D with zero-boundary conditions and $\gamma \in (0,2)$, then the γ-LQG surface associated with h of parameter γ is described by the measure μ_h on D which formally has density $e^{\gamma h}$ with respect to Lebesgue measure. As h is a distribution and does not take values at points, this expression requires interpretation. One can construct this measure rigorously by considering approximations h_ε to h (by averaging the field on circles of radius ϵ) and then take μ_h to be the weak limit as $\varepsilon \to 0$ of $\varepsilon^{\gamma^2/2} e^{h_\varepsilon(z)} dz$ where dz denotes Lebesgue measure on D; see [16]. If one has two planar domains D_1, D_2, a conformal transformation $\varphi \colon D_1 \to D_2$, an instance of the GFF h_2 on D_2, and lets

$$(11) \qquad h_1 = h_2 \circ \varphi + Q \log |\varphi'| \quad \text{where} \quad Q = \frac{2}{\gamma} + \frac{\gamma}{2}$$

then the γ-LQG measure μ_{h_2} associated with h_2 is a.s. the image under φ of the γ-LQG measure μ_{h_1} associated with h_1. A *quantum surface* is an equivalence class of fields h where we say that two fields are equivalent if they are related as in (11).

This construction generalizes to any law on fields h which is absolutely continuous with respect to the GFF. The results in this article will be related to two such laws [64, 14]:

1. The γ-quantum cone (an infinite-volume surface).
2. The γ-LQG sphere (a finite-volume surface).

We explain how they can both be constructed with the ordinary GFF h as the starting point.

The γ-quantum cone can be constructed by the following limiting procedure starting with an instance of the GFF h as above. Fix a constant $C > 0$ and note that adding C to h has the effect of multiplying areas as measured by μ by the factor $e^{\gamma C}$. If one samples $z \in D$ according to μ and then rescales the domain so that the mass assigned by μ_{h+C} to $B(z,1)$ is equal to 1 then the law one obtains in the $C \to \infty$ limit is that of a γ-quantum cone. (The construction given in [64, 14] is more direct in the sense that a precise recipe is given for sampling from the law of the limiting field.) That is, a γ-quantum cone is the infinite-volume γ-LQG surface which describes the local behavior of an γ-LQG surface near a μ_h-typical point.

The (unit area) γ-LQG sphere can also be constructed using a limiting procedure using the ordinary GFF h as above as the starting point. This

construction works by first fixing $C > 0$ large, $\epsilon > 0$ small, and then *conditioning* on the event that the amount of mass that μ assigns to D is in $[e^{\gamma C}, e^{\gamma(C+\epsilon)}]$, so that the amount mass assigned to D by μ_{h-C} is in $[1, e^{\gamma \epsilon}]$, then sends first $C \to \infty$ and then $\epsilon \to 0$. (The constructions given in [14, 49] are more direct because they involve precise recipes for sampling from the law of the limiting h.) One can visualize this construction by imagining that conditioning the area to be large (while keeping the boundary values of h constrained to be 0) leads to the formation of large a bubble. In the $C \to \infty$ limit, the opening of the bubble (which is the boundary of the domain) collapses to a single point, and it turns out that this point is typical (i.e., conditioned on the rest of the surface its law is given by that of the associated γ-LQG measure).

In [14, 49], it is shown that it is possible to represent various types of γ-LQG surfaces (cones, spheres, and disks) decorated by an independent SLE as a gluing of a pair of continuous trees. We first explain a version of this construction in which $\gamma = \sqrt{2}$ and the surface is a unit-area LQG sphere decorated with an independent SLE$_8$. Let X and Y be independent one-dimensional Brownian excursions parameterized by $[0, 1]$. Let C be large enough so that the graphs of X and $C - Y$ are disjoint, as illustrated in Figure 6. We define an equivalence relation $\sim$ on the rectangle $R = [0, 1] \times [0, C]$ by declaring to be equivalent points which lie on either:

1. horizontal chords either entirely below the graph of X or entirely above graph of $C - Y$ (green lines in Figure 6), or
2. vertical chords between the graphs of X and $C - Y$ (red lines in Figure 6).

We note that under $\sim$, all of ∂R is equivalent so we may think of $\sim$ as an equivalence relation on the two-dimensional sphere $\mathbb{S}^2$. It is elementary to check using Moore's theorem [56] (as explained in [14, Section 1.1]) that almost surely the topological structure associated with $R/\sim$ is homeomorphic to $\mathbb{S}^2$. This sphere comes with additional structure, namely:

1. a space-filling path[3] η' (corresponding to the projection of the path which follows the red lines in Figure 6 from left to right), and
2. a measure μ (corresponding to the projection of Lebesgue measure on $[0, 1]$).

We refer to this type of structure as a *peanosphere*, as it is a topological sphere decorated with a path which is the peano curve associated with a

---

[3]As explained just below, η' is related to an SLE$_{\kappa'}$ curve with $\kappa' > 4$. We use the convention here from [50, 51, 52, 55], which is to use a prime whenever $\kappa' > 4$.

space-filling tree.

The peanosphere associated with the pair (X, Y) does not *a priori* come with an embedding into the Euclidean sphere $\mathbb{S}^2$. However, it is shown in [14, 49] that there is a canonical embedding (up to Möbius transformations) of the peanosphere associated with (X, Y) into $\mathbb{S}^2$, which is measurable with respect to (X, Y). This embedding equips the peanosphere with a conformal structure. The image of μ under this embedding is a $\sqrt{2}$-LQG sphere, see [14, 49] as well as [11, 5]), and the law of the space-filling path η' is the following natural version of SLE$_8$ in this context [55]: If we parameterize the $\sqrt{2}$-LQG sphere by the Riemann sphere $\widehat{\mathbb{C}}$, then η' is equal to the weak limit of the law of an SLE$_8$ on $B(0, n)$ from $-in$ to in with respect to the topology of local uniform convergence when parameterized by Lebesgue measure. (The construction given in [55] is different and is based on the GFF.) The random path η' and the random measure μ are coupled together in a simple way. Namely, given μ, one samples from the law of the path by first sampling an SLE$_8$ (modulo time parameterization) independently of μ and then reparameterizing it according to μ-area (so that in t units of time it fills t units of μ-area).

This construction generalizes to all values of $\kappa' \in (4, \infty)$. In the more general setting, we have that $\gamma = \sqrt{\kappa}$ where $\kappa = 16/\kappa' \in (0, 4)$, and the pair of independent Brownian excursions is replaced with a continuous process (X, Y) from $[0, 1]$ into $\mathbb{R}^2_{\geq 0}$ which is given by the linear image of a two-dimensional Brownian excursion from the origin to the origin in the Euclidean wedge of opening angle

$$\theta = \frac{\pi \gamma^2}{4} = \frac{\pi \kappa}{4} = \frac{4\pi}{\kappa'}$$

see [14, 49, 21]. (In the infinite-volume version of the peanosphere construction, the Brownian excursions (X, Y) are replaced with Brownian motions, and the corresponding underlying quantum surface is a γ-quantum cone [14].)

The main results of [14, 49] imply that the information contained in the pair (X, Y) is a.s. *equivalent* to that of the associated SLE$_{\kappa'}$-decorated γ-LQG surface. More precisely, the map f from SLE$_{\kappa'}$-decorated γ-LQG surfaces to Brownian excursions is almost everywhere well-defined and almost everywhere invertible, and both f and f^{-1} are measurable.

The peanosphere construction leads to a natural topology on surfaces which can be represented as a gluing of a pair of trees (a space-filling tree and a dual tree), as illustrated in Figure 6. Namely, such a tree-decorated surface is encoded by a pair of continuous functions (X, Y) where X (resp.

Y) is given by the interface function of the tree (resp. dual tree) on the surface. We recall that the interface function records the distance of a point on the tree to the root when one traces its boundary with unit speed. We emphasize that both continuum and discrete tree-decorated surfaces can be described in this way. In the case of a planar map, we view each edge as a copy of the unit interval and use this to define "speed." Equivalently, one can consider the discrete-time interface function and then extend it to the continuum using piecewise linear interpolation. Applying a rescaling to the planar map corresponds to applying a rescaling to the discrete pair of trees, hence their interface functions. If we have two tree-decorated surfaces with associated pairs of interface functions (X, Y) and (X', Y'), then we define the distance between the two surfaces simply to be the sup-norm distance between (X, Y) and (X', Y').

The peanosphere approach to SLE/LQG convergence (i.e., identifying a natural pair of trees in the discrete model and proving convergence in the topology where two configurations are close if their tree interface functions are close) was introduced in [65, 14] to deal with infinite-volume limits of FK-cluster-decorated random planar maps, which correspond to $\kappa \in [2, 4)$ and $\kappa' \in (4, 8)$. Extensions to the finite volume case and a "loop structure" topology appear in [22, 33, 32, 24].

Since bipolar-oriented planar maps converge in the peanosphere topology to SLE_{12}-decorated $\sqrt{4/3}$-LQG, we conjecture that they also converge in other natural topologies, such as

- The *conformal path topology* defined as follows. Assume we have selected a method of "conformally embedding" discrete planar maps in the sphere. (This might involve circle packing, Riemann uniformization, Tutte embedding, or some other method.) Then the green path in Figure 2 becomes an actual path: a function η_n from $[0, 1]$ to the unit sphere (where n is the number of lattice steps) parameterized so that at time k/n the path finishes traversing its kth edge. An SLE_{12}-decorated $\sqrt{4/3}$-LQG sphere can be described similarly by letting η be the SLE path parameterized so that a t fraction of LQG volume is traversed between times 0 and t. (Note that the parameterized path η encodes both the LQG measure *and* the SLE path.) The conformal path topology is the uniform topology on the set of paths from $[0, 1]$ to the sphere. The conjecture is that η_n converges to η weakly w.r.t. the uniform topology on paths. See [16, 64] for other conjectures of this type. Recently, the first convergence statement of this type was proved for the so-called "mated-CRT maps" using the Tutte embedding in [31].

- The Gromov–Hausdorff–Prokhorov–uniform topology on metric measure spaces decorated with a curve. So far, convergence in this topology has only proved in the setting of a uniformly random planar map decorated by a self-avoiding walk (SAW) to SLE$_{8/3}$ on $\sqrt{8/3}$-LQG in [23, 25, 26] and and also decorated by a percolation to SLE$_6$ on $\sqrt{8/3}$-LQG [29, 27, 30, 28]. These works use as input the convergence of uniformly random planar maps to the Brownian map [43, 45] and the construction of the metric space structure of $\sqrt{8/3}$-LQG [54, 46, 47, 53, 48, 49]. It is still an open problem to endow γ-LQG with a canonical metric space structure for $\gamma \neq \sqrt{8/3}$ and to prove this type of convergence result for random planar maps with other models from statistical physics.

An interesting problem which illustrates some of the convergence issues that arise is the following: In the discrete setting, the interface functions between the NW and SE trees determine the bipolar map which in turn determine the interface functions between the NE and SW trees. Likewise, in the continuous setting, the interface functions (a Brownian excursion) between the NW and SE trees a.s. determine the SLE-decorated LQG which in turn a.s. determine the interface function (another Brownian excursion) between the NE and SW trees.

CONJECTURE 4.4. *The joint law of both NW/SE and NE/SW interface functions of a random bipolar-oriented planar map converges to the joint law of both NW/SE and NE/SW interface functions of* SLE$_{12}$*-decorated* $\sqrt{4/3}$*-LQG.*

One might expect to be able to approximate the discrete NW/SE interface function with a continuous function, obtain the corresponding continuous NE/SW function, and hope that this approximates the discrete NE/SW function. One problem with this approach is that while the maps f^{-1} and f are measurable, they are (presumably almost everywhere) discontinuous, so that even if two interface functions are close, it does not follow that the corresponding measures and paths are close. However, since Brownian excursions are random perturbations rather than "worst case" perturbations of random walk excursions, we expect the joint laws to converge despite the discontinuities of f and f^{-1}.

Update: Conjecture 4.4 has been proven in [34].

5. Open question. In addition to questions regarding strengthening the topology of convergence, which are discussed at the end of Section 4.2,

it would be interesting to extend the theory to other surface graphs, such as the torus, or a disk with four boundary vertices which are alternately source, sink, source, sink.

REFERENCES

[1] Aaron Abrams and Richard Kenyon. Fixed-energy harmonic functions, 2015. arXiv:1505.05785.

[2] David Aldous. The continuum random tree. I. *Ann. Probab.*, 19(1):1–28, 1991.

[3] David Aldous. The continuum random tree. II. An overview. In *Stochastic analysis*, London Math. Soc. Lecture Note Ser. #167, pages 23–70. Cambridge Univ. Press, 1991.

[4] David Aldous. The continuum random tree. III. *Ann. Probab.*, 21(1):248–289, 1993.

[5] Juhan Aru, Yichao Huang, and Xin Sun. Two perspectives of the 2D unit area quantum sphere and their equivalence, 2015. arXiv:1512.06190.

[6] Nicolas Bonichon, Mireille Bousquet-Mélou, and Éric Fusy. Baxter permutations and plane bipolar orientations. *Sém. Lothar. Combin.*, 61A:Article B61Ah, 2009/11.

[7] Mireille Bousquet-Mélou. Counting planar maps, coloured or uncoloured. In *Surveys in combinatorics 2011*, London Math. Soc. Lecture Note Ser. #392, pages 1–49. Cambridge Univ. Press, 2011.

[8] John Cardy. SLE for theoretical physicists. *Ann. Physics*, 318(1):81–118, 2005.

[9] Dmitry Chelkak, Hugo Duminil-Copin, Clément Hongler, Antti Kemppainen, and Stanislav Smirnov. Convergence of Ising interfaces to Schramm's SLE curves. *C. R. Math. Acad. Sci. Paris*, 352(2):157–161, 2014.

[10] Robert Cori and Bernard Vauquelin. Planar maps are well labeled trees. *Canad. J. Math.*, 33(5):1023–1042, 1981.

[11] François David, Antti Kupiainen, Rémi Rhodes, and Vincent Vargas. Liouville quantum gravity on the Riemann sphere. *Comm. Math. Phys.*, 342(3):869–907, 2016. arXiv:1410.7318.

[12] Hubert de Fraysseix, Patrice Ossona de Mendez, and Pierre Rosenstiehl. Bipolar orientations revisited. *Discrete Appl. Math.*, 56(2-3):157–179, 1995.

[13] Julien Dubédat. Duality of Schramm–Loewner evolutions. *Ann. Sci. Éc. Norm. Supér. (4)*, 42(5):697–724, 2009.

[14] B. Duplantier, J. Miller, and S. Sheffield. Liouville quantum gravity as a mating of trees, 2014. arXiv:1409.7055.

[15] Bertrand Duplantier. Random walks and quantum gravity in two dimensions. *Phys. Rev. Lett.*, 81(25):5489–5492, 1998.

[16] Bertrand Duplantier and Scott Sheffield. Liouville quantum gravity and KPZ. *Invent. Math.*, 185(2):333–393, 2011.

[17] J. Duraj and V. Wachtel. Invariance principles for random walks in cones, 2015. arXiv:1508.07966.

[18] Stefan Felsner, Éric Fusy, Marc Noy, and David Orden. Bijections for Baxter families and related objects. *J. Combin. Theory Ser. A*, 118(3):993–1020, 2011.

[19] Éric Fusy, Dominique Poulalhon, and Gilles Schaeffer. Bijective counting of plane bipolar orientations and Schnyder woods. *European J. Combin.*, 30(7):1646–1658, 2009.

[20] Rodolphe Garbit. Brownian motion conditioned to stay in a cone. *J. Math. Kyoto Univ.*, 49(3):573–592, 2009.

[21] E. Gwynne, N. Holden, J. Miller, and X. Sun. Brownian motion correlation in the peanosphere for $\kappa > 8$, 2015. To appear in *Ann. Inst. Henri Poincaré Probab. Stat.* arXiv:1510.04687.

[22] E. Gwynne, C. Mao, and X. Sun. Scaling limits for the critical Fortuin–Kasteleyn model on a random planar map I: cone times, 2015. arXiv:1502.00546.

[23] E. Gwynne and J. Miller. Convergence of the self-avoiding walk on random quadrangulations to SLE$_{8/3}$ on $\sqrt{8/3}$-Liouville quantum gravity, 2016.

[24] E. Gwynne and J. Miller. Convergence of the topology of critical Fortuin–Kasteleyn planar maps to that of CLE$_\kappa$ on a Liouville quantum surface, 2016. In preparation.

[25] E. Gwynne and J. Miller. Metric gluing of Brownian and $\sqrt{8/3}$-Liouville quantum gravity surfaces, 2016.

[26] E. Gwynne and J. Miller. Scaling limit of the uniform infinite half-plane quadrangulation in the Gromov–Hausdorff–Prokhorov-uniform topology, 2016.

[27] E. Gwynne and J. Miller. Characterizations of SLE$_\kappa$ for $\kappa \in (4, 8)$ on Liouville quantum gravity, 2017.

[28] E. Gwynne and J. Miller. Chordal SLE$_6$ explorations of a quantum disk, 2017.

[29] E. Gwynne and J. Miller. Convergence of percolation on uniform quadrangulations with boundary to SLE$_6$ on $\sqrt{8/3}$-Liouville quantum gravity, 2017.

[30] E. Gwynne and J. Miller. Convergence of the free Boltzmann quadrangulation with simple boundary to the Brownian disk, 2017.

[31] E. Gwynne, J. Miller, and S. Sheffield. The Tutte embedding of the mated-CRT map converges to Liouville quantum gravity, 2017.

[32] E. Gwynne and X. Sun. Scaling limits for the critical Fortuin–Kastelyn model on a random planar map III: finite volume case, 2015. arXiv:1510.06346.

[33] E. Gwynne and X. Sun. Scaling limits for the critical Fortuin–Kastelyn model on a random planar map II: local estimates and empty reduced word exponent. *Electron. J. Probab.*, 22:paper no. 45, 56 pp., 2017. arXiv:1505.03375.

[34] Ewain Gwynne, Nina Holden, and Xin Sun. Joint scaling limit of a bipolar-oriented triangulation and its dual in the peanosphere sense, 2016. arXiv:1603.01194.

[35] Ewain Gwynne, Adrien Kassel, Jason Miller, and David B. Wilson. Active spanning trees with bending energy on planar maps and SLE-decorated Liouville quantum gravity for $\kappa > 8$, 2016. arXiv:1603.09722.

[36] Adrien Kassel and David B. Wilson. Active spanning trees and Schramm–Loewner evolution. *Phys. Rev. E*, 93:062121, 2016.

[37] Richard W. Kenyon, Jason Miller, Scott Sheffield, and David B. Wilson. Six-vertex model and Schramm–Loewner evolution. *Phys. Rev. E*, 95:052146, 2017. arXiv:1605.06471.

[38] Gregory F. Lawler, Oded Schramm, and Wendelin Werner. The dimension of the planar Brownian frontier is 4/3. *Math. Res. Lett.*, 8(4):401–411, 2001.

[39] Gregory F. Lawler, Oded Schramm, and Wendelin Werner. Values of Brownian intersection exponents. I. Half-plane exponents. *Acta Math.*, 187(2):237–273, 2001.

[40] Gregory F. Lawler, Oded Schramm, and Wendelin Werner. Values of Brownian intersection exponents. II. Plane exponents. *Acta Math.*, 187(2):275–308, 2001.

[41] Gregory F. Lawler, Oded Schramm, and Wendelin Werner. Values of Brownian inter-
     section exponents. III. Two-sided exponents. *Ann. Inst. H. Poincaré Probab. Statist.*,
     38(1):109–123, 2002.

[42] Gregory F. Lawler, Oded Schramm, and Wendelin Werner. Conformal invariance
     of planar loop-erased random walks and uniform spanning trees. *Ann. Probab.*,
     32(1B):939–995, 2004.

[43] Jean-François Le Gall. Uniqueness and universality of the Brownian map. *Ann.
     Probab.*, 41(4):2880–2960, 2013.

[44] A. Lempel, S. Even, and I. Cederbaum. An algorithm for planarity testing of graphs.
     In *Theory of Graphs (Internat. Sympos., Rome, 1966)*, pages 215–232. 1967.

[45] Grégory Miermont. The Brownian map is the scaling limit of uniform random plane
     quadrangulations. *Acta Math.*, 210(2):319–401, 2013.

[46] J. Miller and S. Sheffield. An axiomatic characterization of the Brownian map, 2015.
     arXiv:1506.03806.

[47] J. Miller and S. Sheffield. Liouville quantum gravity and the Brownian map I: The
     QLE(8/3,0) metric, 2015. arXiv:1507.00719.

[48] J. Miller and S. Sheffield. Liouville quantum gravity and the Brownian map III: the
     conformal structure is determined, 2016.

[49] Jason Miller and Scott Sheffield. Liouville quantum gravity spheres as matings of
     finite-diameter trees, 2015. arXiv:1506.03804.

[50] Jason Miller and Scott Sheffield. Imaginary geometry I: Interacting SLEs. *Probab.
     Theory Related Fields*, 164(3-4):553–705, 2016.

[51] Jason Miller and Scott Sheffield. Imaginary geometry II: reversibility of $\mathrm{SLE}_\kappa(\rho_1; \rho_2)$
     for $\kappa \in (0, 4)$. *Ann. Probab*, 44(3):1647–1722, 2016.

[52] Jason Miller and Scott Sheffield. Imaginary geometry III: reversibility of SLE_κ for
     $\kappa \in (4, 8)$. *Ann. of Math. (2)*, 184(2):455–486, 2016.

[53] Jason Miller and Scott Sheffield. Liouville quantum gravity and the Brownian map
     II: geodesics and continuity of the embedding, 2016. arXiv:1605.03563.

[54] Jason Miller and Scott Sheffield. Quantum Loewner evolution. *Duke Math. J.*,
     165(17):3241–3378, 2016. arXiv:1312.5745.

[55] Jason Miller and Scott Sheffield. Imaginary geometry IV: interior rays, whole-plane
     reversibility, and space-filling trees. *Probab. Theory Related Fields*, published online,
     to appear in print, 2017. arXiv:1302.4738.

[56] R. L. Moore. Concerning upper semi-continuous collections of continua. *Trans. Amer.
     Math. Soc.*, 27(4):416–428, 1925.

[57] R. C. Mullin. On the enumeration of tree-rooted maps. *Canad. J. Math.*, 19:174–183,
     1967.

[58] Steffen Rohde and Oded Schramm, 2002. Private communication.

[59] Gilles Schaeffer. *Conjugaison d'arbres et cartes combinatoires aléatoires*. PhD thesis,
     Université Bordeaux I, 1998.

[60] Oded Schramm. Scaling limits of loop-erased random walks and uniform spanning
     trees. *Israel J. Math.*, 118:221–288, 2000.

[61] Oded Schramm and Scott Sheffield. Contour lines of the two-dimensional discrete
     Gaussian free field. *Acta Math.*, 202(1):21–137, 2009.

[62] Oded Schramm and Scott Sheffield. A contour line of the continuum Gaussian free
     field. *Probab. Theory Related Fields*, 157(1-2):47–80, 2013.

[63] Scott Sheffield. Exploration trees and conformal loop ensembles. *Duke Math. J.*, 147(1):79–129, 2009.

[64] Scott Sheffield. Conformal weldings of random surfaces: SLE and the quantum gravity zipper. *Ann. Probab.*, 44(5):3474–3545, 2016. arXiv:1012.4797.

[65] Scott Sheffield. Quantum gravity and inventory accumulation. *Ann. Probab.*, 44(6):3804–3848, 2016. arXiv:1108.2241.

[66] Scott Sheffield and Wendelin Werner. Conformal loop ensembles: the Markovian characterization and the loop-soup construction. *Ann. of Math. (2)*, 176(3):1827–1917, 2012.

[67] Michio Shimura. Excursions in a cone for two-dimensional Brownian motion. *J. Math. Kyoto Univ.*, 25(3):433–443, 1985.

[68] Stanislav Smirnov. Critical percolation in the plane: conformal invariance, Cardy's formula, scaling limits. *C. R. Acad. Sci. Paris Sér. I Math.*, 333(3):239–244, 2001.

[69] Stanislav Smirnov. Conformal invariance in random cluster models. I. Holomorphic fermions in the Ising model. *Ann. of Math. (2)*, 172(2):1435–1467, 2010.

[70] W. T. Tutte. A census of planar maps. *Canad. J. Math.*, 15:249–271, 1963.

[71] W. T. Tutte. Chromatic sums for rooted planar triangulations: the cases $\lambda = 1$ and $\lambda = 2$. *Canad. J. Math.*, 25:426–447, 1973.

[72] Dapeng Zhan. Duality of chordal SLE. *Invent. Math.*, 174(2):309–353, 2008.